Heat and Mass Transfer During Microwave-Convective Drying

Stefan J. Kowalski, Grzegorz Musielak, and Jacek Banaszak
Dept. of Process Engineering, Institute of Technology and Chemical Engineering, Poznań University of Technology, Poznań 60-965, Poland

DOI 10.1002/aic.11948
Published online August 24, 2009 in Wiley InterScience (www.interscience.wiley.com)

The article presents a mathematical model of drying that describes the kinetics of combined microwave-convective drying for the process as a whole. Based on this model, the drying curves and the temperature evolutions of the drying body were constructed by a number of computer-simulated drying programs, which were chosen to follow the respective experimental processes carried out on a cylindrical sample made of kaolin. The experimental data allowed both the estimate of material coefficients arising in the model and the validation of the theory. A very satisfactory correlation of the theoretical predictions with the experimental data is found. The main novelty of this article is the mathematically complete drying model that describes all periods of the microwave-convective drying process. Application of such a complete model is necessary if we want to optimize drying processes with respect to drying time and consumption of energy via computer simulations. © 2009 American Institute of Chemical Engineers *AIChE J,* 56: 24–35, 2010
Keywords: heat transfer, mass transfer, drying, microwave heating, convective transport, numerical analysis, experimental validation

Introduction

Various materials that undergo drying in industrial production require different approach to this process. In many cases, the time of drying becomes important because of the production rate. In another case, the time is less important but the quality of the products, that is, their appearance and good mechanical state or the biological value in the case of food or medicine products are relevant. In all cases, important is the minimization of the energy use as drying is a big energy consuming process. To fulfill these requirements, one has to look for special methods of drying among others for the combined methods in which different sources of energy supply are used.

The main aim of this article is to present the mathematical model of microwave-convective drying and its experimental validation. The theoretical and experimental studies based on this model may show that combined drying processes being consisted of different methods of drying may bring very positive results as it concerns shortening of drying time as the good quality of dried products

Modeling of drying processes, and in particular combined processes, is relevant to the development of fast and energy save drying processes and has been treated widely during the last decade. The paper by Zhang et al.[1] presents a review of microwave-related drying methods for fruit and vegetables. Combined drying methods like convective-microwave,[2–18] convective-microwave-infrared,[19] microwave-vacuum,[20,21] microwave-infrared,[22,23] solar,[24] and other methods[25–29] have been proposed to improve the effectiveness of drying, i.e., to minimize the drying time and the consumption of energy as well as to improve the quality of the dried products. The variety of these drying methods is wide, but, however, they do not embrace the drying kinetics for the process as a whole, which is treated in this article.

Proper design of hybrid drying processes has to satisfy a number of requirements. In particular, the design needs to optimize the complex process and provide suitable control.

Correspondence concerning this article should be addressed to S. J. Kowalski at Stefan.J.Kowalski@put.poznan.pl

© 2009 American Institute of Chemical Engineers

The optimization procedure must be based on the actual drying model, reflecting the drying process as a whole. Construction of a coherent model for hybrid processes is a very difficult as the mechanisms of moisture transport vary not only between processes but also during different periods in a given process.

In an earlier paper,[30] experimental validation of a heat and mass transfer model for convective drying only was presented. The main aim of this article is to present a mathematical model reflecting the kinetics of combined microwave-convective drying for the process as a whole. First, a number of experimental tests of this kind of drying were carried out to provide data for the whole drying kinetics process. The experimental data indicated the nature of the assumptions appropriate for a simplified mathematical model. Next, based on this model, a number of computer-simulated tests were performed with various programs of drying, and the theoretical results were compared with the experimental data to demonstrate the good correlation.

An effort is made to model completely the kinetics of the combined microwave-convective drying and less attention is devoted to the mechanical aspect of drying-like deformations and drying-induced stresses. The influence of the drying body deformation on the heat and mass transfer is neglected, so the theory is applicable only to materials that deform very little during drying. A cylindrically shaped sample made of kaolin was used in both experimental and theoretical studies. The experimental data provided estimates of the material coefficients in the mathematical model and also demonstrated consistency with the theory. Temperature and moisture distributions, and their time evolution, calculated numerically from the mathematical model, compared closely with the experimental results for different drying programs.

Materials and Methods

In this section, the kinetics of the microwave-convective drying is inferred from experimental studies, suggesting suitable simplifying assumptions for a mathematical theory. The experimental tests were carried out on cylindrical samples made of KOC kaolin clay produced by the SURMIN-KAOLIN S.A. company. The chemical composition and physical properties of the KOC kaolin are given in Table 1.

The kaolin prepared for the experiments was mixed with water to get a greasy paste of initial moisture content approximately $X_0 = 0.45$ (kg water/kg dry kaolin). Next, the paste was stored in a closed box for 48 h for homogenization of the moisture distribution. The material was then used to mold a series of similar cylindrical samples of radius $R = 0.03$ m and height $H = 0.06$ m.

The microwave-convective drying experiments were carried out in a laboratory chamber dryer WS 110 manufactured by the PLASMATRONICA firm. The dimensions of the working chamber were as follows: 300 × 400 × 450 mm (height × breadth × depth). The power-controlled range was upto a maximum of 600 W. A distinct series of experiments was performed for microwave powers of 120, 180, and 240 W. The samples dried at a power of 180 W cracked, and those dried at a power of 240 W split completely, so the useful drying experiments were carried out at a continuous irradiating power of 120 W. The air from surrounding

Table 1. Specification of Kaolin at 12% Moisture Content

		KOC
Chemical composition	SiO_2 (%)	51.9
	Al_2O_3 (%)	33.9
	Others (%)	14
Mineral composition	Kaolinite (%)	80
	Illite (%)	9
	Quarz (%)	9
	Others (%)	2
R_r—strength of the kaolin	Formed samples (Pa)	7×10^5
Shrinkage of drying (110°C)	(%)	2.4

having temperature ca. 22°C was supplied to the microwave dryer with the help of mechanical ventilation system installed in the dryer. The air temperature T_a and the air relative humidity φ_a were measured at the outlet of the dryer. The temperature of the sample during drying was measured on the sample surface by an infrared thermometer installed on the top surface of the microwave chamber dryer. Figure 1 presents the experimental set-up for the process.

The experiments were carried out in two steps. First, the drying curves and the change of surface temperature of the sample were measured, and second, the final distribution of temperature inside the material was determined by cutting the sample and using the thermovision camera (Figure 1b).

During the first step, the kaolin sample was placed on a ceramic plate supported on an electronic balance WPS 2100/C made by the RADWAG firm. The balance registered the mass of moisture removal every each minute with an accuracy of 0.01 g. The decrease of moisture mass in the drying sample vs. time (drying curves) for different power of the microwave heater is presented in Figure 2a. In drying with power of 120 W (curve 1 in Figures 2a,b), the air temperature supplied from the surrounding was ca. 22°C and relative humidity ca. 45%. The air relative humidity and temperature measured at the outlet of the dryer changed from ca. 44% to 24% and 23 to 48°C, respectively. The infrared pirometer measured the temperature of the sample surface, and its variation in time presents the curve in Figure 2b.

During the second step, three groups of samples, each one of four units, were dried in several processes. The individual samples were taken out of the dryer after scheduled time of 1, 2, 3, 4 min (first series), after 5, 10, 15, 30 min (second series), and after 60, 120, 180, 240 min (final series), and placed in a special PCV form to cut along the cylinder generating line (Figure 1b) and take infrared pictures of the sample cross sections with a Therma CAM B2 camera made by the FLIR SYSTEMS firm. Figure 3a illustrates the distribution of temperature in the middle cross section of the cylindrical sample after 30 min of microwave-convective drying, and Figure 3b presents for comparison an equivalent picture for convective drying.

It is seen that the greatest temperature by microwave-convective drying appears in the middle of the cylinder, whereas by convective drying it is at the middle point of the bottom surface, which is heated from below and moisture efflux is prevented.

More details concerning experimental studies for convective drying are presented by Kowalski et al.[30] and Musielak and Banaszak.[31]

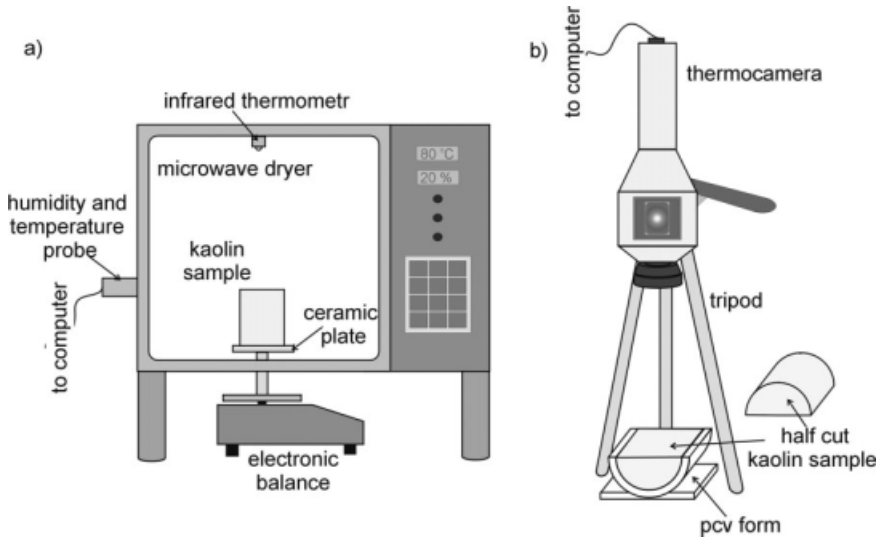

Figure 1. The experimental set-up: (a) microwave-convective dryer and (b) determination of the temperature distribution.

Modeling approach

Underpinning the drying model are the balances of mass, linear momentum, angular momentum, energy, entropy, and the principles of irreversible thermodynamics. Such theories have been presented by Kowalski[32,33] and Kowalski et al.,[30] but here some modifications are introduced to extend to a complete microwave-convective drying process.

The present model of drying incorporates the following assumptions:

The drying material consists of three phases: solid skeleton, liquid, and gas in pores, which are represented by α phase mass content X^{α} (dry basis) and a phase volume fraction ϕ^{α} (alpha = s-solid, l-liquid, g-gas), which are continuous functions of space and time due to an averaging procedure applied to the representative volume element (RVE)[34,35]).

The skeleton is a deformable body; however, the deformations are assumed to be sufficiently small to neglect in the numerical treatments of heat and mass transfer.

The theory excludes thermal shocks, and therefore, some dynamic terms (accelerations, inertia forces, kinetic energy, etc.) are neglected in the balance equations.

The viscous stress deviator in the moisture is neglected, being much smaller than the stress deviator of the solid skeleton.

The skeleton of the material (dry body) has dielectric properties.

The only effect of microwaves acting on the material is that they generate heat inside the material.

Local thermal equilibrium between moisture and the skeleton is assumed, so that their temperatures at each point are equal.

The balance equations are formulated in Euler's description by using the spatial rectangular coordinates $\boldsymbol{x}\{x, y, z\}$, and in the frame reference of solid skeleton have the general form as follows[33]:

$$\frac{\partial \psi^{\alpha}}{\partial t} + \nabla \cdot (\psi^{\alpha} \boldsymbol{v}^{s}) = \nabla \cdot [\boldsymbol{f}^{\alpha} - \psi^{\alpha}(\boldsymbol{v}^{\alpha} - \boldsymbol{v}^{s})] + b^{\alpha} + \hat{\overline{p}}^{\alpha} \quad (1)$$

where Table 2 presents definition of ψ^{α} for the specific balances. Here, u^{α} and s^{α} denote the specific internal energy and entropy of constituent α; $\boldsymbol{\sigma}^{\alpha}$, ρ^{α}, $\boldsymbol{q}^{\alpha}$, r^{α}, denote the partial stress tensors, the partial densities, the heat flux vectors, and the volumetric heat supply, and $\hat{\rho}^{\alpha}$, $\hat{m}^{\alpha}$, $\hat{e}^{\alpha}$, and $\hat{s}^{\alpha}$ denote the

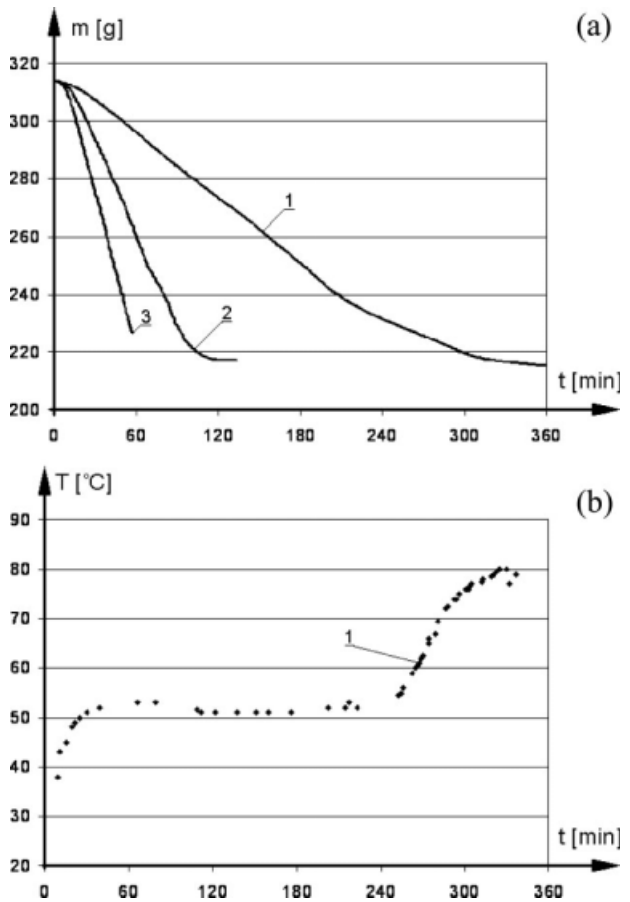

Figure 2. The experimental drying kinetics: (a) drying curves: 1—120 W, 2—180 W, 3—240 W and (b) temperature evolution on the sample surface: 1—120 W.

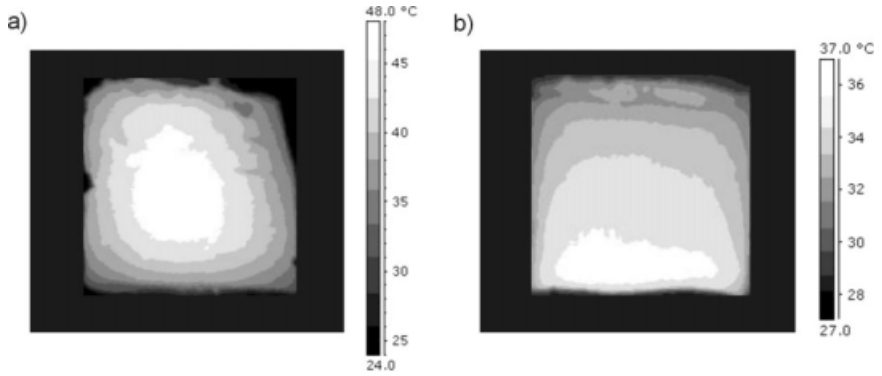

Figure 3. Distribution of the temperature in the cylindrical samples: (a) microwave-convective drying and (b) convective drying.

production terms of mass, momentum, energy, and entropy, for constituent α respectively, and g and T denote the gravity acceleration and temperature.

Total mass, momentum, and energy of a multicomponent medium have to be conserved. These laws of conservation are as follows[36]:

$$\sum_{\alpha} \hat{\rho}^{\alpha} = 0, \quad \sum_{\alpha} \hat{m}^{\alpha} = 0, \quad \sum_{\alpha} \hat{e}^{\alpha} = 0. \tag{2}$$

Drying processes are irreversible, so the total entropy production obeys the second law of thermodynamics; that is,

$$\rho^{s}\dot{s} + \nabla \cdot \left(\frac{\boldsymbol{q}}{T} + \sum_{\alpha} s^{\alpha} \boldsymbol{J}^{\alpha} \right) - \frac{\Re}{T} = \sum_{\alpha} \hat{s}^{\alpha} \geq 0 \tag{3}$$

where $s = s^{s} + X^{l}s^{l} + X^{g}s^{g}$ denotes the total entropy of the body per unit mass of the skeleton, $X^{\alpha} = \rho^{\alpha}/\rho^{s}$ is the constituent mass content (dry basis), $\boldsymbol{q}$ is the sum of constituent fluxes $\boldsymbol{q}^{\alpha}$, $\boldsymbol{J}^{\alpha}$ is the flux of constituent mass with respect to the skeleton, and $\mathfrak{R}$ is the total volumetric heat supply to the control volume (sum of constituent terms $\rho^{\alpha}r^{\alpha}$). The expression in brackets is the total entropy supplied to the body due to both heat conduction and heat transported by mass fluxes. Dot over a symbol denotes the time derivative with solid convection velocity $\boldsymbol{v}^{s}$.

The balance (1) for the energy with the conservation laws (2) is as follows:

$$\rho^{s}\dot{u} = \boldsymbol{\sigma} \cdot \boldsymbol{d} + \sum_{\alpha} \left[\rho^{s}\mu^{\alpha}\dot{X}^{\alpha} - \boldsymbol{J}^{\alpha} \cdot (\nabla\mu^{\alpha} - \boldsymbol{g}) - \mu^{\alpha}\hat{\rho}^{\alpha} \right] - \nabla \cdot \left(\boldsymbol{q} + T \sum_{\alpha} s^{\alpha}\boldsymbol{J}^{\alpha} \right) + \Re \tag{4}$$

where $u = u^{s} + X^{l}u^{l} + X^{g}u^{g}$ denotes the total internal energy of the body per unit mass of the skeleton, $\boldsymbol{\sigma}$ is the total stress tensor (sum of partial stress tensors), $\boldsymbol{d}$ is the strain rate tensor of the solid skeleton, and μ^{α} is the chemical potential of constituent α (α = l, g). In (4), the balance equation for total momentum was used and the constituent accelerations were neglected as insignificant in a drying processes; that is,

$$\nabla \cdot \boldsymbol{\sigma} + \rho\boldsymbol{g} \approx 0 \quad \text{with} \quad \boldsymbol{\sigma} = \sum_{\alpha} \boldsymbol{\sigma}^{\alpha} \quad \text{and} \quad \rho = \sum_{\alpha} \rho^{\alpha} \tag{5}$$

The strain rate tensor and the chemical potential are defined as follows:

$$\boldsymbol{d} = \frac{1}{2}\left[\nabla \boldsymbol{v}^{s} + (\nabla \boldsymbol{v}^{s})^{T} \right] \quad \text{and} \quad \mu^{\alpha} = u^{\alpha} - P^{\alpha}/\rho^{\alpha} - s^{\alpha}T \tag{6}$$

where $\boldsymbol{v}^{s}$ denotes the velocity of the solid skeleton. Here, $\boldsymbol{\sigma}^{\alpha} = P^{\alpha}\boldsymbol{I}$ (α = l, g), where $\boldsymbol{I}$ is the unit tensor and P^{α} the partial pressure of constituent α, since the stress deviators of liquid and gas are neglected.

The mass of the skeleton in the control volume is conserved ($\hat{\rho}^{s} = 0$), so that the skeleton mass balance is as follows:

$$\dot{\rho}^{s} + \rho^{s}\nabla \cdot \boldsymbol{v}^{s} = 0 \tag{7}$$

The local mass balance for the moisture is fundamental to developing the differential equation governing the moisture content distribution. From (1) and (7),

$$\rho^{s}\dot{X}^{\alpha} = -\nabla \cdot \boldsymbol{J}^{\alpha} + \hat{\rho}^{\alpha} \quad \text{with} \quad \hat{\rho}^{l} + \hat{\rho}^{g} = 0 \tag{8}$$

The entropy inequality (3), after applying the energy balance (4), becomes as follows:

$$-\rho^{s}\left(\dot{f} + s\dot{T}\right) + \boldsymbol{\sigma} \cdot \boldsymbol{d} + \sum_{\alpha} \left[\rho^{s}\mu^{\alpha}\dot{X}^{\alpha} - \boldsymbol{J}^{\alpha} \cdot (\nabla\mu^{\alpha} - \boldsymbol{g}) - \mu^{\alpha}\hat{\rho}^{\alpha} \right] - \left(\boldsymbol{q} + T \sum_{\alpha} s^{\alpha}\boldsymbol{J}^{\alpha} \right) \cdot \frac{\nabla T}{T} \geq 0 \tag{9}$$

where $f = u - sT$ denotes the free internal energy of the body per unit mass of the skeleton.

Table 2. Components of the Individual Balance Equations

Balance	ψ^{α}	f^{α}	b^{α}	$*p^{\alpha}$
Mass	ρ^{α}	0	0	$*\rho^{\alpha}$
Momentum	$\rho^{\alpha}\boldsymbol{v}^{\alpha}$	$\boldsymbol{\sigma}^{\alpha}$	$\rho^{\alpha}\boldsymbol{g}$	$*m^{\alpha}$
Energy	$\rho^{\alpha}u^{\alpha}$	$\boldsymbol{\sigma}^{\alpha} \cdot \boldsymbol{v}^{\alpha} - \boldsymbol{q}^{\alpha}$	$\rho^{\alpha}\,(r^{\alpha} + \boldsymbol{g} \cdot \boldsymbol{v}^{\alpha})$	$*e^{\alpha}$
Entropy	$\rho^{\alpha}s^{\alpha}$	$-\boldsymbol{q}^{\alpha}/T$	$\rho^{\alpha}r^{\alpha}/T$	$*s^{\alpha}$

The thermodynamic inequality (9) constitutes a constraint helpful for developing the rate equations for heat and mass transfer. We assume that drying processes run in the neighborhood of thermodynamic equilibrium, so Gibbs' equation applies, which here has the form,

$$\dot{f} = -s\dot{T} + \frac{1}{\rho^{s}}\sigma \cdot \boldsymbol{d} + \sum_{\alpha} \mu^{\alpha}\dot{X}^{\alpha} \tag{10}$$

Now, the inequality (9) with Gibbs' Equation (10) and mass conservation (8) reduces to

$$-\sum_{\alpha} \boldsymbol{J}^{\alpha} \cdot (\nabla\mu^{\alpha} - \boldsymbol{g}) - \hat{\rho}^{l}\left(\mu^{l} - \mu^{g}\right) - \left(\boldsymbol{q} + T\sum_{\alpha} s^{\alpha}\boldsymbol{J}^{\alpha}\right) \cdot \frac{\nabla T}{T} \geq 0 \tag{11}$$

The inequality (11) expresses the entropy production from the energy dissipated during heat and mass transfer processes. Recalling the Curie-Prigogine symmetry principle, and identifying the respective thermodynamic forces responsible for the heat and mass transfer, it follows that[37]

$$-\hat{\rho}^{l}\left(\mu^{l} - \mu^{g}\right) \geq 0 \tag{12}$$

$$-\boldsymbol{J}^{\alpha} \cdot (\nabla\mu^{\alpha} - \boldsymbol{g}) \geq 0 \tag{13}$$

$$-\left(\boldsymbol{q} + T\sum_{\alpha} s^{\alpha}\boldsymbol{J}^{\alpha}\right) \cdot \frac{\nabla T}{T} \geq 0 \tag{14}$$

The constrains (12)–(14) imply specific forms for the thermodynamic fluxes, namely

$$\hat{\rho}^{l} = -\hat{\rho}^{g} = -\varpi\left(\mu^{l} - \mu^{g}\right) \quad \text{with} \quad \varpi \geq 0 \tag{15}$$

$$\boldsymbol{J}^{\alpha} = -\Lambda^{\alpha}(\nabla\mu^{\alpha} - \boldsymbol{g}) \quad \text{with} \quad \Lambda^{\alpha} \geq 0 \tag{16}$$

$$\boldsymbol{q} = -\lambda\nabla T - T\sum_{\alpha} s^{\alpha}\boldsymbol{J}^{\alpha} \quad \text{with} \quad \lambda \geq 0 \tag{17}$$

The above rate equations constitute sufficient conditions (not necessary) to satisfy the thermodynamic constraints. The coefficients of mass and heat transfer, ϖ, Λ^{α}, and λ, are in general function of the state variables.

Relation (15) shows that the rate of phase transition from liquid to vapor is proportional to the difference between chemical potentials μ^{l} and μ^{g}. Thermodynamic equilibrium (i.e., the absence of phase transition) requires these two potentials to be equal. In this relation ϖ is termed the phase transition coefficient.

The gradient of the chemical potential μ^{α}, and the gravity force per unit mass $\boldsymbol{g}$ (the derivative of the gravity potential: $\boldsymbol{g} = -\nabla\mu^{grav}$), constitute the thermodynamic forces for moisture flow. In relation (16), Λ^{α} is the moisture transport coefficient (mobility parameter). Based on Gibbs' Equation (10), the chemical potential is the derivative of the free energy with respect to the constituent mass content; that is,

$$\mu^{\alpha} = \left(\frac{\partial f}{\partial X^{\alpha}}\right)_{T,\varepsilon,X^{\beta\neq\alpha}} = \mu^{\alpha}\left(T, \varepsilon, X^{l}, X^{g}\right) \tag{18}$$

Developing the above state equation with respect to the parameters of state (temperature T, volumetric strain ε, mass contents X^{α}), and defining the respective derivatives as material coefficients, gives the physical relation for the chemical potentials μ^{α} (α = l and g). As the chemical potentials are intensive parameters, they must be homogeneous functions of degree zero with respect to the mass fractions; that is,

$$\mu^{\alpha}\left(T, \varepsilon, nX^{l}, nX^{g}\right) = n^{k}\mu^{\alpha}\left(T, \varepsilon, X^{l}, X^{g}\right) \tag{19}$$

where n is an arbitrary parameter, and $k = 0$ for homogeneous functions of degree zero. Differentiating both sides of this equation with respect to n and substituting $n = 1$, we obtain the Gibbs-Duhem relation[38]

$$\frac{\partial\mu^{\alpha}}{\partial X^{l}}X^{l} + \frac{\partial\mu^{\alpha}}{\partial X^{g}}X^{g} = 0 \quad \text{for} \quad \alpha = \text{l and g} \tag{20}$$

Such a homogeneous system of equations has a nontrivial solution only if the main determinant is equal to zero. This implies that the potentials μ^{l} and μ^{g} are related. This is an important conclusion that will be used for modeling the phase transitions of liquid into vapor inside the drying body.

The total heat flux expressed by relation (17) consists of the heat conducted to the moist porous body (being proportional to the gradient of temperature assuming Fourier's law) and of the heat transported with the mass flux $\boldsymbol{J}^{\alpha}$ (heat convection); λ is the coefficient of thermal conductivity (a material constant).

The local balance of energy (4) constitutes the basis for developing the differential equation for heat transfer. Substituting Gibbs' Equation (10) and the rate equations (15)–(17) into balance (4), we get the following:

$$\rho^{s}\dot{s}T = \nabla \cdot (\lambda\nabla T) + Q^{*} + \Re \tag{21}$$

where Q^{*} denotes the internal source of heat coming from energy dissipated during irreversible processes. This quantity can be considered very small in comparison to the heat supplied to the body due to external convective or microwave heating and is therefore not given explicitly.

The coefficient of heat conduction is assumed to be an average of heat conduction through the skeleton and the moisture; that is,

$$\lambda = (1-\phi)\lambda^{s} + \phi S\lambda^{l} = (1-\phi)\left(\lambda^{s} + \frac{\rho^{sr}}{\rho^{lr}}X^{l}\lambda^{l}\right) \tag{22}$$

where λ^{s} and λ^{l} are the coefficients of heat conduction for skeleton and liquid, $S = \phi^{l}/\phi$ means saturation, ϕ is the porosity, and ρ^{sr} and ρ^{lr} are the real densities of solid and liquid.

The total entropy is the sum of that for skeleton and moisture, and its time derivative is as follows:

$$\dot{s}\left(T,\varepsilon,X^{\mathrm{l}},X^{\mathrm{g}}\right)=\frac{c_{\mathrm{v}}}{T}\dot{T}+\gamma^{(T)}\dot{\varepsilon}+s^{\mathrm{l}}\dot{X}^{\mathrm{l}}+s^{\mathrm{g}}\dot{X}^{\mathrm{g}} \tag{23}$$

where $c_{\mathrm{v}}=c_{\mathrm{v}}^{\mathrm{s}}+c_{\mathrm{v}}^{\mathrm{l}}X^{\mathrm{l}}+c_{\mathrm{v}}^{\mathrm{g}}X^{\mathrm{g}}\approx c_{\mathrm{v}}^{\mathrm{s}}+c_{\mathrm{v}}^{\mathrm{l}}X^{\mathrm{l}}$ is the specific heat of the multicomponent body.

The volumetric strain rate $\dot{\varepsilon}$ is assumed to be very small, with negligible influence on the changes of entropy and temperature, so it is neglected.

Equation (21) with subject to (23), (8), and (15) becomes the following:

$$\rho^{\mathrm{s}}c_{\mathrm{v}}\dot{T}=\nabla\cdot(\lambda\nabla T)-\varpi\left(\mu^{\mathrm{l}}-\mu^{\mathrm{g}}\right)l+\Re \tag{24}$$

where $l=T(s^{\mathrm{g}}-s^{\mathrm{l}})$ denotes the latent heat of evaporation, and the expression $T(s^{\mathrm{l}}\nabla\cdot\boldsymbol{J}^{\mathrm{l}}+s^{\mathrm{g}}\nabla\cdot\boldsymbol{J}^{\mathrm{g}})$ describing the change of heat due to moisture compression has been neglected in (24) as small in comparison to the term containing the latent heat of evaporation and the other terms.

The term $\mathfrak{R}$ expressing the volumetric heat supply due to absorption of microwave energy depends on the loss factor and microwave frequency. It has been shown (see e.g.,[15,19,39–43]) that microwave power converted into heat per unit volume of material is equal to the product of electric conductivity σ^* and the square of the electric field intensity $\boldsymbol{E}$, that is,[33]

$$\Re=\frac{1}{2}\alpha^{*}\boldsymbol{E}^{2}=\frac{1}{2}\omega\varepsilon''\boldsymbol{E}_{0}^{2}\exp(-2\delta\,\mathbf{x}\cdot\boldsymbol{n}) \tag{25}$$

Summarizing the above:

The amount of microwave energy absorbed by drying material decays exponentially with distance, as determined by the parameter δ, which depends on the dielectric properties of the medium: loss factor ε'' and microwave frequency ω.

The absorption of microwave energy depends primarily on the amount of water content; however, energy can also be absorbed by the skeleton, if it consists of bound (structural) water or other molecules of polar character.

The above statement suggests introducing a linear dependency of the absorbed microwave energy on the moisture content by the following:

$$\frac{1}{2}\omega\varepsilon''\boldsymbol{E}_{0}^{2}=\rho^{\mathrm{s}}(A+BX^{\mathrm{l}}) \tag{26}$$

where A and B express the amount of microwave energy absorbed by the skeleton and moisture, respectively.

The final expression for the microwave heat source is proposed to be

$$\Re=\rho^{\mathrm{s}}(A+BX^{\mathrm{l}})\exp(-2\delta\,\boldsymbol{x}\cdot\boldsymbol{n}) \tag{27}$$

Equation (27) shows that the microwave heat source may not disappear completely for a dry body; that is, when the free water is removed from the material.

The local mass balance (8) is the basis for a differential equations for mass transfer. Substituting the moisture flux (16) and the rate of mass change due to phase transition (15), we obtain the following:

$$\rho^{\mathrm{s}}\dot{X}^{\mathrm{l}}=\nabla\cdot\left\lfloor\Lambda^{\mathrm{l}}(\nabla\mu^{\mathrm{l}}-\boldsymbol{g})\right\rfloor-\varpi\left(\mu^{\mathrm{l}}-\mu^{\mathrm{g}}\right) \tag{28}$$

$$\rho^{\mathrm{s}}\dot{X}^{\mathrm{g}}=\nabla\cdot\left\lfloor\Lambda^{\mathrm{g}}(\nabla\mu^{\mathrm{g}}-\boldsymbol{g})\right\rfloor+\varpi\left(\mu^{\mathrm{l}}-\mu^{\mathrm{g}}\right) \tag{29}$$

As stated earlier, the chemical potentials μ^{l} and μ^{g} are functions of the state variables $\{T,\ \varepsilon,\ X^{\mathrm{l}},\ X^{\mathrm{g}}\}$. We now introduce some simplifications. The first one follows from the observation and statement that the amount of liquid, and not gas, determines the material dryness and shrinkage. By drying in moderate conditions, gas flows freely out of the body and has no (or insignificant) influence on the thermomechanical state of the dried material. Therefore, only the balance (28) is relevant, whereas (29) is redundant. This does not mean that the phase transition of liquid into vapor is meaningless. It influences significantly the energy balance because of the latent heat of evaporation, as it is evident in the differential Equation (24) for heat transfer. Another simplification follows from neglecting volumetric strain ε as small for kaolin (ca. 2.5 to 6%) and insignificant for the moisture transfer.

It is known that in each thermodynamic equilibrium state the chemical potentials of liquid and vapor are equal, i.e., $\mu^{\mathrm{l}}|_{\mathrm{e}}=\mu^{\mathrm{g}}|_{\mathrm{e}}$. Recalling the Gibbs-Duhem relation (13), we assume the following relation between the chemical potentials of vapor and liquid:

$$\mu^{\mathrm{g}}-\mu^{\mathrm{g}}|_{\mathrm{e}}=\left[1-a(T,X^{\mathrm{l}})\right]\left(\mu^{\mathrm{l}}-\mu^{\mathrm{l}}\big|_{\mathrm{e}}\right) \tag{30}$$

where $0\le a\le 1$ is the phase transition efficiency (at thermodynamic equilibrium: $a=0$).

The rate Equation (16) can now be rewritten as follows:

$$\boldsymbol{J}^{\mathrm{l}}=-\Lambda^{\mathrm{l}}\left(c_{\mathrm{T}}\nabla T+c_{\mathrm{X}}\nabla X^{\mathrm{l}}-\boldsymbol{g}\right) \tag{31}$$

where coefficients c_{T} and c_{X} are equal to the derivatives of chemical potential μ^{l}, the former with respect to temperature at constant liquid content (thermodiffusion), and the latter with respect to liquid content at constant temperature (diffusion).

Gravity forces are neglected as insignificant in drying of small cylindrical sample. Substituting relation (30) into the balance (28) and expanding the chemical potential μ^{l} in a Taylor's series in the vicinity of the equilibrium state (reference state), the differential Equation (28) for liquid transfer becomes the following:

$$\rho^{\mathrm{s}}\dot{\theta}=\nabla\cdot\left[\Lambda^{\mathrm{l}}\nabla(c_{\mathrm{T}}\vartheta+c_{\mathrm{X}}\theta)\right]-\quad\varpi a(c_{\mathrm{T}}\vartheta+c_{\mathrm{X}}\theta) \tag{32}$$

where $\vartheta=T-T_{\mathrm{e}}$ and $\theta=X^{\mathrm{l}}-X_{\mathrm{e}}^{\mathrm{l}}$ denote the departure of temperature and liquid content from the equilibrium state in a local sense.[37]

In drying, there are two main periods: the constant drying rate period (CDRP) and the falling drying rate period (FDRP).[44,45] For the purpose of mathematical modeling, it is important to note that these two periods of drying are characterized by different mechanisms of moisture transport. The drying rate during CDRP is independent of time. In this period, the moisture is transported as liquid from the body interior toward the body surface where it evaporates just as from

an open surface of liquid. In this stage, the amount of evaporated liquid inside the body is insignificant in comparison to that evaporated at the body surface, so that the parameter of phase transition efficiency can be taken as $a \approx 0$. The body reaches a stable distribution of temperature and (32) then becomes simply the diffusion equation. The FDRP begins when the body surface dries in some places and the liquid menisci in capillaries start to penetrate the body. The local moisture content close to the body surface reaches a critical value X_{cr}. The rate of evaporation decreases beyond X_{cr} and the temperature of the body rises above the wet bulb temperature prescribed to the CDRP, and tends to the air temperature T_a. More and more liquid evaporates inside the body. To account for this change of mechanism of moisture transfer between the CDRP and the FDRP, we postulate the following form for the moisture transport coefficient Λ^l (see also[46,47])

$$\Lambda^l = \frac{\sigma(T)}{\eta(T)} f(X^l) \quad \text{with} \quad \frac{f(X^l)}{f_0} = \begin{cases} 1 & \text{for} \quad X^l \geq X_{cr} \\ \left(\frac{X^l - X_e}{X_{cr} - X_e}\right)^2 & \text{for} \quad X_e \leq X^l \leq X_{cr} \end{cases} \tag{33}$$

where σ and η are the surface tension and the viscosity of moisture, respectively, f_0 is a structural parameter of the moisture transport influencing the permeability of porous body, and X_e is the moisture content at which the transport of moisture in the form of liquid is stopped.

The phase transition inside the body is controlled by the parameter of phase transition efficiency a, which has distinct partitions:

$$\frac{a}{a_{ef}} = \begin{cases} 0 & \text{for} \quad X^l \geq X_{cr} \\ 1 - \left(\frac{X^l - X_e}{X_{cr} - X_e}\right)^2 & \text{for} \quad X_e \leq X^l \leq X_{cr} \\ \left(\frac{X^l}{X_e}\right)^2 & \text{for} \quad 0 \leq X^l \leq X_e \end{cases} \tag{34}$$

where a_{ef} is the effective value of the phase transition efficiency. This partitioned form of parameter allows numerical programming of the drying process as a whole. Note that the absence of phase transitions in the CDRP is assumed for $X \geq X_{cr}$. The phase transition inside the body starts to increase, and the diffusional moisture transport starts to decrease, in the FDRP, i.e., when $X_e \leq X^l \leq X_{cr}$. When the moisture content at the surface reaches the equilibrium value with the ambient air X_e, transport of liquid stops totally, and the rest of liquid inside the body is removed due to evaporation and diffusion of vapor.

The experimental tests and numerical calculations were performed on a kaolin cylindrical samples of radius $R = 0.03$ m and height $H = 0.06$ m, placed on impermeable plates. The distribution and time evolution of moisture content and temperature were determined for both the CDRP and the FDRP. Equations (24) and (32) in cylindrical coordinates take the form as follows:

$$\rho^s \dot{\theta} = \nabla \cdot \left[\Lambda^l \nabla (c_T \vartheta + c_X \theta)\right] - \varpi a (c_T \vartheta + c_X \theta) \tag{35}$$

$$\rho^s c_v \dot{\vartheta} = \nabla \cdot (\lambda \nabla \vartheta) - l \varpi a (c_T \vartheta + c_X \theta) + \Re \tag{36}$$

where $\nabla = \frac{\partial}{\partial r} \boldsymbol{i}_r + \frac{\partial}{\partial z} \boldsymbol{i}_z$ and $\nabla \cdot \nabla = \frac{\partial^2}{\partial r^2} + \frac{1}{r}\frac{\partial}{\partial r} + \frac{\partial^2}{\partial z^2}$.

The experimental tests on microwave-convective drying indicated the greatest increase of temperature occurs in the middle of the cylinder. This means that microwave damping is not strong in the kaolin cylinder, otherwise the temperature maximum would be elsewhere. Therefore, for numerical calculations, we neglect the damping term in Eq. (27) and assume the microwave heat source to be a linearly dependent on the moisture content; that is,

$$\Re = \rho^s \left(A + B X^l\right) \tag{37}$$

The boundary conditions for mass and heat transfer for drying of the cylinder with bottom surface insulated for moisture outflow are as follows:

$$-\Lambda^l \nabla (c_T \vartheta + c_X \theta)|_{\partial B} \cdot \boldsymbol{n} = k_m (\mu^v|_{\partial B} - \mu_a) \tag{38a}$$

$$\lambda \nabla \vartheta|_{\partial B} \cdot \boldsymbol{n} = h_T (\vartheta_a - \vartheta|_{\partial B}) - l k_m (\mu^v|_{\partial B} - \mu_a) \tag{38b}$$

$$\frac{\partial \theta}{\partial r}|_{r=0} = 0, \quad c_X \frac{\partial \theta}{\partial z}|_{z=0} = -c_T \frac{\partial \vartheta}{\partial z}|_{z=0} \tag{38c}$$

$$\frac{\partial \vartheta}{\partial r}|_{r=0} = 0, \quad \frac{\partial \vartheta}{\partial r}|_{z=0} = h_{T0} (\vartheta_a - \vartheta|_{z=0}) \tag{38d}$$

where ∂B denotes the upper and the lateral surfaces of the cylinder (not insulated), and $h_{T0} = 0.96 h_T$ in Eq. (38d). This difference in the coefficients of convective heat exchange was introduced to take into account the conduction resistance of the ceramic plate. The initial conditions express the uniform distribution of moisture content and temperature at the beginning of drying; that is,

$$\theta(r,z,t)|_{t=0} = \theta_0 = \text{const.} \quad \vartheta(r,z,t)|_{t=0} = \vartheta_0 = \text{const} \tag{38e}$$

In the above conditions, $\mu^v|_{\partial B}$ and μ_a denote the chemical potentials of vapor at the boundary surface and in the core of drying air, θ_0 and ϑ_0 are the initial moisture content and initial temperature, and k_m and h_T are the coefficients of convective vapor and heat exchange between the drying body and the air, respectively.

The chemical potential for vapor in air outside the cylinder is the sum of pore vapor potential $\mu^{\otimes}$ and the additional term coming from the mole vapor fraction in air[38]

$$\mu^v(p,T,x) = \mu^{\otimes}(p,T) + R^v T \ln x \tag{39}$$

where R^v is the vapor gas constant, T the temperature, $x = \varphi p^{vs}/p$ the mole fractions of vapor in air, φ is the relative humidity of air, p^{vs} is the partial pressure of saturated vapor, and p the total pressure of air, respectively. The chemical potential for vapor at the cylinder surface changes when the

Table 3. The Constants Evolving in the Drying Model

Partial density of the skeleton	ρ^s	kg/m^3	2300
Volume porosity	ϕ	1	0.5
Thermal conductivity of the skeleton material	λ^s	W/m K	1.78
Thermal conductivity of liquid	λ^l	W/m K	0.597
Specific heat of the skeleton material	c_v^s	J/kg K	728.5
Specific heat of liquid	c_v^l	J/kg K	4180
Moisture contents coefficient of the moisture potential	c_X	m^2/s^2	1.11×10^6
Temperature coefficient of the moisture potential	c_T	m^2/s^2 K	6.3×10^2
Critical moisture contents	X_{cr}	kg$_w$/kg$_s$	0.12
Equilibrium moisture contents	X_e	kg$_w$/kg$_s$	0.04
Constant describing the structural parameters of kaolin (Eq. 33)	f_0	kg s^2/m^4	6×10^{-7}
The effective phase efficiency (Eqs. 34, 35, 36)	ϖa_{ef}	kg s/m^5	2.5×10^{-6}
Constant describing the absorption of microwave energy by skeleton (Eq. 37)	A	J/m^3 s	126
Constant describing the absorption of microwave energy by moisture (Eq. 37)	B	J/m^3 s	20

vapor–liquid interface recedes into the body. Therefore, we reformulate the convective term for vapor transfer on the right hand side of boundary conditions (38a) and (38b). We state that the relative humidity of air close to the material surface is a function of the material moisture content at the boundary $X^l|_{\partial B}$; that is,

$$\varphi|_{\partial B} = \begin{cases} 1 & \text{for } X^l\big|_{\partial B} \geq X_{cr} \\ 1 - \frac{1-\varphi_a}{X_{cr}-X_e}\left(X_{cr} - X^l\big|_{\partial B}\right) & \text{for } X_{cr} \geq X^l\big|_{\partial B} \geq X_e \end{cases} \quad (40)$$

Thus, we assume that the vapor is saturated at the surface when the moisture content of the body is greater than critical and is unsaturated when the moisture content is less than critical. Such a form of driving force for vapor transfer allows us to control the drying process by suitable choice of the air parameters T_a and φ_a. Using the expression (39) for the chemical potential of vapor in air, the difference in vapor potentials at the surface and in ambient air is as follows[32,48]:

$$\mu^v|_{\partial B} - \mu_a = s^v\left(T_a - T|_{\partial B}\right) + R^v\left[T|_{\partial B}\left(\ln\varphi|_{\partial B}\frac{p^{vs}|_{\partial B}}{p}\right) - T_a\left(\ln\varphi_a\frac{p_a^{vs}}{p}\right)\right] \quad (41)$$

where s^v is the entropy of vapor at the average temperature from T_a and $T|_{\partial B}$.

Results and Discussion

The aim of this section is to compare the drying kinetics obtained from the numerical simulations with the experimental data. The experimental data obtained for a drying process carried out at temperature 41.5°C were used for estimating the coefficient for heat and mass transfer which arises in the mathematical model (Table 3).

The various thermal coefficients for water, water vapor, and moist air were adopted from,[44,49,50] tabulated between 0 and 100°C in steps of 1 degree. The coefficients of convective vapor transfer k_m, (38a, b,) and convective heat transfer h_T, (38b) were estimated on the basis of experiments carried out at air temperature $T_a = 41.5$°C and air humidity at the initial stage equal to $\varphi_a = 30.57\%$.[31,51,52] The numerical calculations of the drying curves, temperature evolutions, and distributions of moisture content and temperature in the cylindrical sample for different temperatures and relative humidity of drying air were then performed with these estimated coefficients.

The numerical simulations of drying kinetics require the solution of a two-dimensional initial boundary value problem formulated by the system of differential equations (35) and (36) that include the microwave heat source (37), boundary conditions (38a)–(38d), together with the expressions (40) and (41), and the homogeneous initial conditions for moisture and temperature distribution (38e). The numerical problem is solved by an explicit finite difference method. The spatial mesh consists of 101 × 51 points. Stability requires the time step during the calculations to be less then 0.33 s, and the time step 0.01 s was used. During the FDRP, the moisture transfer coefficient Λ^l and the difference of potentials ($\mu^v|_{\partial B} - \mu_a$) is strongly dependent on temperature and on the moisture content at the cylinder surface $X|_{\partial B}$. The nonlinearity in the governing equations and boundary conditions also can lead to instability of a numerical algorithm, prevented here by using a special algorithm.[53]

Figure 4a presents the drying curves and Figure 4b the temperature evolution in time for microwave-convective drying acquired experimentally and numerically.

The vertical axis in Figure 4a measures total mass of the dried sample and indirectly the moisture content that changes during drying. The dotted line in Figure 4b illustrates the change of temperature on the sample surface measured by an infrared thermometer installed in the dryer chamber. The solid lines present the numerically simulated temperature and its evolution at several points of the cylinder, as shown in the right corner of Figure 4b. It is seen that the temperatures at several points differ significantly from each other. The highest temperature is in the middle of the cylinder (point 2). The lowest is at the cylinder corner where the removal of moisture is the most intensive. The numerically simulated temperature on the cylinder surface (point 4) is the closest to that measured experimentally.

Figure 5 presents the distribution of temperature simulated numerically in the cylinder in a 30 min microwave-convective drying process, which is equivalent to that in Figure 3a determined experimentally.

Comparing the curves in Figures 5 and 3a, the qualitative similarity of the experimentally determined temperature distribution with that predicted theoretically can be seen. There is, however, a difference in the magnitude of the

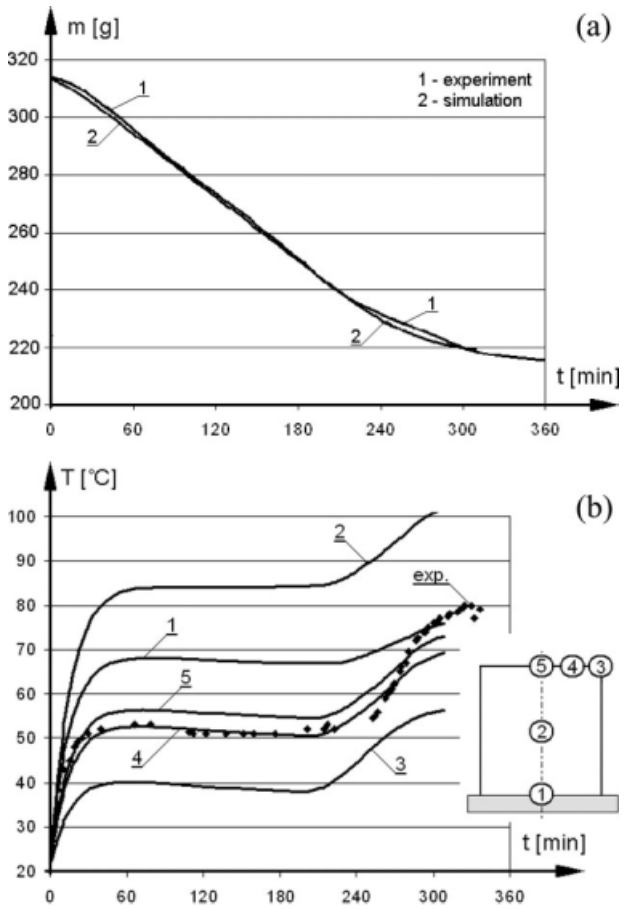

Figure 4. Microwave-convective drying: (a) drying curves and (b) temperature vs. time.

temperatures presented in these figures. This discrepancy follows from the inevitable cooling of the sample after taking it out of the dryer and cutting it for the photography with thermovision camera (Figure 1b). A better comparison of the temperature distributions in the cylinder is given by the spatial distributions. Figures 6a,b illustrate the numerically simulated spatial distributions of temperature in the cylinder (equivalent to that in Figure 5) at some instances of the CDRP and the FDRP.

Figures 3a (experimental) and 5, 6a and 6b (theory) clearly show that the maximum temperature, both in the CDRP and the FDRP, is around the middle of the cylinder, and the minimum is at the surface, in particular, at the cylinder upper corner. This minimum at the top corner follows from the facts that first, the greatest energy is escaping with vapor just from the top corner, and second, the amount of moisture is the lowest at the corner and the intensity of microwave heating is proportional to the moisture content.

The maximum temperature around the middle of the cylinder results from the volumetric mechanism of heat supply by microwave irradiation. To include this effect in our model, the radiation term $\mathfrak{N}$ expressed by formula (37) was inserted into the equation of balance of energy (1) (in final form Eq. (36)).

The equivalent distribution of temperature in the cylinder in convective drying (for example, Kowalski et al.[30]) is quite different than that in microwave-convective drying. In

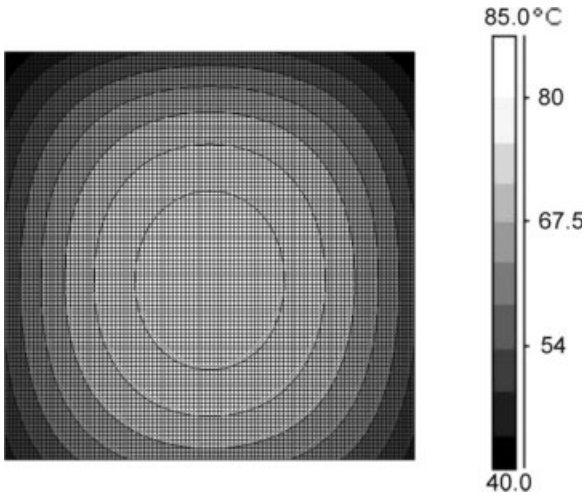

Figure 5. Numerically simulated distribution of temperature in the cylinder during microwave-convective drying.

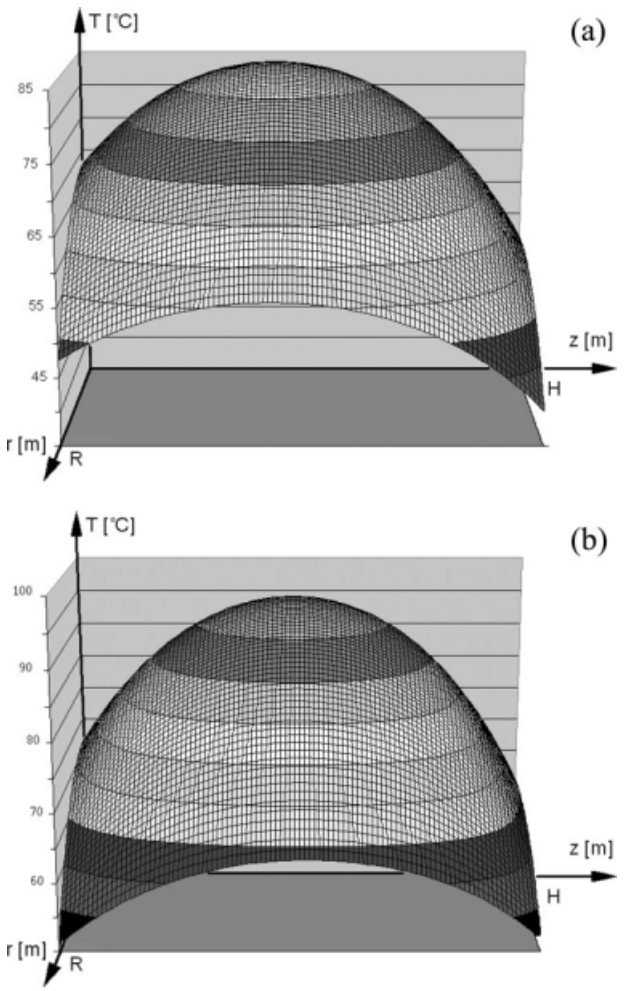

Figure 6. Distribution of temperature in microwave-convective drying: (a) CDRP and (b) FDRP.

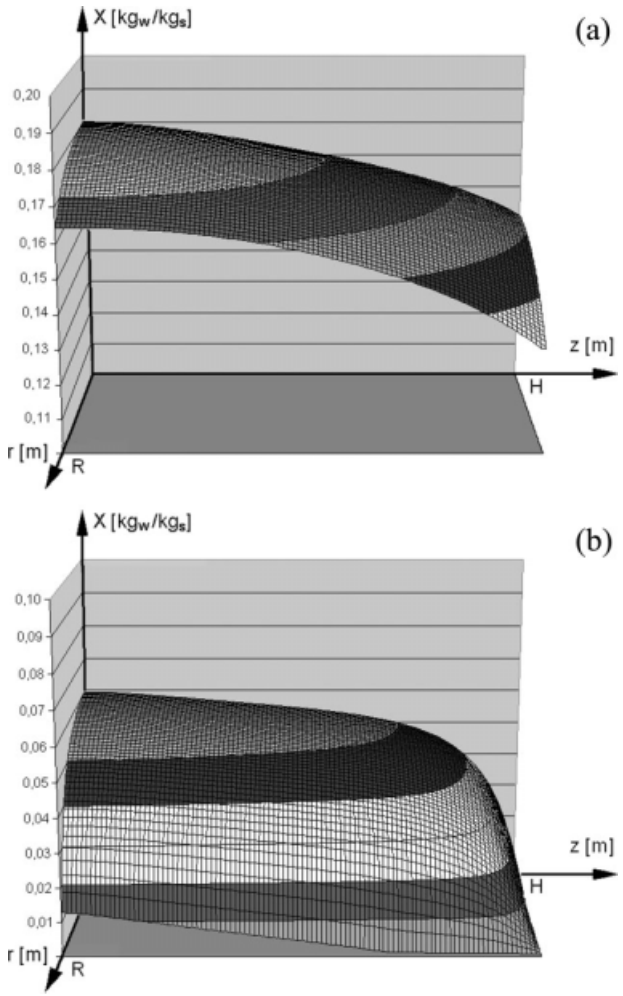

Figure 7. Distribution of moisture content in microwave-convective drying: (a) CDRP and (b) FDRP.

convective drying, the highest temperature is at the bottom surface of the cylinder, which is hydro-isolated, so that drying does not proceed there. The lowest temperature is on the upper surface, which is dried the most intensively. The sample temperature starts to rise when the FDRP begins, first at the upper and the side surfaces of the sample.

The distribution of temperature gained in microwave-convective drying is very profitable for moisture transport, in particular in the CDRP. Namely, in such a temperature distribution, the diffusional and thermodiffusional fluxes coincide, in contradictory to pure convective drying where they are of opposite directions. Thus, we may expect an easier removal of moisture in microwave-convective then in pure convective drying, and it really is. We may notice this as on drying curves (Figure 2a) as on the plots presenting moisture distribution.

Figures 7a,b illustrate the distribution of the moisture content in the cylinder during microwave-convective drying in the CDRP and the FDRP.

The maximum moisture content is at the middle point of the bottom surface of the cylinder, which is insulated (ceramic plate), whereas the minimum is at the top corner, where free mass transfer takes place. The values of moisture content in the CDRP are greater than those in the FDRP but more uniformly distributed throughout the cylinder. We may state that in the microwave-convective drying, the gradients of moisture distribution are significantly smaller than those in pure convective drying,[30] what may follow just from the synergy of diffusion and thermodiffusion mechanisms. This conclusion is of great importance when the mechanical effects accompanying drying are analyzed. Namely, it is known that a nonlinear distribution of moisture is a friendly condition for nonuniform shrinkage and stress generation.[32] The greater are the gradients in moisture distribution the greater stresses may arise.

The error between the experimental and the numerical results is defined as the ratio of the difference of the experimental and the numerical results at a given instant of time, to the difference between the initial and the final values, namely[31]

$$\Delta_m(t) = \left|\frac{m_{\mathrm{exp}}(t) - m_{\mathrm{sim}}(t)}{m_0 - m_{\mathrm{e}}}\right|. \quad \Delta_T(t) = \left|\frac{T_{\mathrm{exp}}(t) - T_{\mathrm{sim}}(t)}{T_{\mathrm{a}} - T_0}\right|$$

where m denotes the mass and T the temperature of the tested sample. For example, the average relative error Δ_m for the drying curves presented in Figure 4a was below 1.6% and its maximum 2.3%. The average relative error Δ_T for the temperatures shown in Figure 4b (point 4) is from 0.5 to 1.2% during the CDRP, and from 7 to 12% during the FDRP. The deviation of the results rises slightly with increase of the drying temperature. The discrepancies between experimental and computed theoretical results in microwave-convective drying are of similar magnitude to those for pure convective drying.

Conclusions

The results of experimental tests and an outline of a microwave-convective drying theory have been presented. As extensively illustrated, the mathematical drying model reflects very well the kinetics of the microwave-convective drying over the whole range of the process. The drying curves and the time evolution of the dried body temperature, and the distribution of moisture content and temperature in dried body were analyzed. The graphs of the moisture content and temperature evolution are not straight lines, but are complex curves reflecting the changeable drying mechanisms in several stages of drying.

A theory of drying that is able to describe the whole drying process is in general a nonlinear, and the material coefficient appearing in the mathematical model strongly depend on the moisture content and temperature. To include or exclude the dominating individual heat and mass transfer mechanisms during a given period of drying, it is necessary to introduce coefficient functions which change across different ranges, as for example those given by Eqs. (33), (34), or (40).

The most difficult problem in constructing a mathematical model of drying for numerical computation is the determination of the material coefficients in terms of moisture content and temperature. Estimation of these coefficients needs

specific equipment, skill, and a long time to perform the necessary tests. Therefore, only some of these coefficients were established by the authors, and others were constructed from previously published data.

A major effort in this article was experimental validation of the theory. The many graphical comparisons show that the theoretical results reflect qualitatively very well the experimental data and many cases differ only slightly from them. We conclude therefore, that the constructed mathematical model of microwave-convective drying imitates closely the drying process as a whole and is thus a basis for optimization of drying processes.

Acknowledgments

This work was carried out as a part of the research project No 3 T09C 030 28, sponsored by the Polish Ministry of Education and Science.

Notation

a = phase transition efficiency
A, B = constants (Table 2)
c_T = coefficient of thermodiffusion [m^2/s^2 K]
c_X = coefficient of diffusion [m^2/s^2]
$\boldsymbol{d}$ = strain rate tensor [s^{-1}]
k_m = coefficient of convective vapor exchange [kg s/m^4]
h_T = coefficient of convective heat exchange [W/m^2 K]
$\boldsymbol{E}$ = electric intensity [V/m]
f = free energy [J/kg]
$f(X^l)$ = moisture transport parameter [kg s^2/m^4]
$\boldsymbol{g}$ = gravity acceleration [m/s^2]
$\boldsymbol{J}^\alpha$ = mass flux of α-constituent [kg/m^2 s]
H = sample height [m]
l = latent heat of evaporation [J/kg]
p = pressure [Pa]
P^α = partial pressure of α-constituent [Pa]
r, R = sample radius [m]
$\boldsymbol{q}, \boldsymbol{q}^\alpha$ = heat flux, heat flux of α-constituent [W/m^2]
R^v = vapor gas constant [J/mol K]
$\mathfrak{R}$ = volumetric heat supply [W/m^3]
$S = \phi^l/\phi$ = saturation
s, s^α = entropy, entropy of α-constituent [J/kg K]
T = temperature [K]
t = time [s]
u = internal energy [J/kg]
$\boldsymbol{v}^\alpha$ = velocity of α-constituent [m/s]
$X^\alpha = \rho^\alpha/\rho^s$ = constituent mass content
$\boldsymbol{x}(x,y,z)$ = spatial coordinates [m]
x_a, x_n = mole fractions of vapor in air

Greek Symbols

α = constituent (alpha = s-solid, l-liquid, g-gas)
δ = coefficient of microwave damping [m^{-1}]
$\varepsilon^*(\varepsilon', \varepsilon'')$ = magnetic permittivity [F/m]
ε = volumetric strain
λ = coefficient of heat conduction [W/m K]
φ = air relative humidity
ϕ^α, ϕ = volume fraction, porosity
μ^α = chemical potential of α-constituent [J/kg]
$\boldsymbol{\sigma}$ = stress tensor [Pa]
σ^* = electric conductivity [1/Ω]
$\hat{\rho}^\alpha$ = rate of α-constituent mass change by phase transitions [kg/m^3 s]
ω = microwave frequency [rd/s]
ϖ = phase transition coefficient [kg s/m^5]
ρ, ρ^α = density, partial density of α-constituent [kg/m^3]
$\vartheta = T - T_e$ = departure of temperature from the equilibrium state [°C]
$\theta = X^l - X^l_e$ = departure of moisture content from the equilibrium state
Λ^α = mass transport coefficient of α-constituent [kg s/m^3]

Indexes

e = equilibrium
g = gas
l = liquid
v = vapor
s = solid, saturated
T = thermal
X = moist

Literature Cited

1. Zhang M, Tang J, Mujumdar AS, Wang S. Trends in microwave-related drying of fruits and vegetables. *Trends Food Sci Technol*. 2006;17:524–534.
2. Perre P, Turner IW. A complete coupled model of the combined microwave and convective drying of softwood in an oversized waveguide. In: Strumiłło Cz., Pakowski Z., editors. *Proceedings of IDS 1996*, Vol. A., Kraków, Poland, 1996:183–194.
3. Zielonka P, Gierlik E, Matejak M, Dolowy K. The comparison of experimental and theoretical temperature distribution during microwave wood heating. *Holtz als Roh- und Werkstoff*. 1997;55:395–398.
4. Zielonka P, Dolowy K. Microwave drying of spruce: moisture content, temperature, and heat energy distribution. *Forest Prod J*. 1998; 48:77–80.
5. Garcia H, Bueno JL. Improving energy efficiency in combined microwave-convective drying. *Drying Technol*. 1998;16:123–140.
6. Feng H, Tang J, Cavalieri RP, Plumb OA. Heat and mass transport in microwave drying of porous materials in a spouted bed. *AIChE J*. 2001;47:1499–1512.
7. Sanga ECM, Raghavan GSV, Mujumdar AS. Heat and mass transfer during microwave-convection drying of composite materials: simulation with incorporation of shrinkage. In: *Proceedings IADC 2*, Vera Cruz, Mexico, 2001:185–205.
8. Sanga ECM, Mujumdar AS, Raghavan GSV. Simulation of convection-microwave drying for shrinkage material. *Chem Eng Process*. 2002;41:487–499.
9. McMinn WAM, Khraisheh MAM, Magee TRA. Modelling the mass transfer during convective, microwave and combined microwave-convective drying of solid slabs and cylinders. *Food Res Int*. 2003;36:977–983.
10. McMinn WAM, McLoughlin CM, Magee TRA. Microwave-convective drying characteristics of pharmaceutical powders. *Powder Technol*. 2005;153:23–33.
11. Andres A, Bilbao C, Fito P. Drying kinetics of apple cylinders under combined hot air-microwave dehydration. *J Food Eng*. 2004;63: 71–78.
12. Kowalski SJ, Rybicki A. Qualitative aspects of convective and microwave drying of saturated porous materials. *Drying Technol*. 2004;22:1173–1189.
13. Kowalski SJ, Rajewska K, Rybicki A. Mechanical effects in saturated capillary-porous materials during convective and microwave drying. *Drying Technol*. 2004;22:2291–2308.
14. Kowalski SJ, Rajewska K, Rybicki A. Stresses generated during convective and microwave drying. *Drying Technol*. 2005;23:1875–1893.
15. Kowalski SJ, Rajewska K, Rybicki A. *Physical Fundamentals of Microwave Drying*. Poznan, Poland: Poznań University of Technology, 2005:113 (in Polish).
16. Cheng WM, Raghavan GSV, Ngadi M, Wang N. Microwave power control strategies on the drying process II. Phase-controlled and cycle controlled microwave/air drying. *J Food Eng*. 2006;76:195–201.
17. Araszkiewicz M, Koziol A, Lipinska A, Lupinski M. Microwave drying of various shape particles suspended in an air stream. In: Kowalski SJ, editor. *Drying of Porous Materials*. Dordrecht, The Netherlands: Springer, 2007:173.
18. Itaya Y, Uchiyama S, Mori S. Internal heating effect and enhancement of drying of ceramics by microwave heating with dynamic control. In: Kowalski SJ, editor. *Drying of Porous Materials*. Dordrecht, The Netherlands: Springer, 2007:29–42.
19. Salagnac P, Glouannec P, Lecharpentier D. Numerical modelling of heat and mass transfer in porous medium during combined hot air,

infrared and microwave drying. *Int J Heat Mass Transf*. 2004;47: 4479–4489.
20. Sicre N, Jomaa W, Puiggali JR. Microwave vacuum drying for suspension. In: Farkas I, editor, *Proceedings of 15*th *International Drying Symposium* (*IDS*), Vol. B. Budapest, Hungary, 2006:1118–1125.
21. Giri SK, Prasad S. Drying kinetics and rehydration characteristics of microwave-vacuum and convective hot air dried mushrooms. *J Food Eng*. 2007;78:512–521.
22. Glouannec P, Lecharpentier D, Noel H. Experimental survey on the combination of radiating infrared and microwave sources for the drying of porous material. *Appl Therm Eng*. 2002;22:1689–1703.
23. Ratanadecho P, Aoki K, Akahori M. Influence of irradiation time, particle sizes and initial moisture content during microwave drying of multilayered capillary porous materials. *J Heat Transf*. 2002;124:1–11.
24. Bennamoun L, Belharmri A. Numerical simulations of drying under variable external conditions: application to solar drying of seedless grapes. *J Food Eng*. 2006;76:179–187.
25. Lazarenko BR, Grosu FP, Bologa MK. Convective heat-transfer enhancement by electric fields. *Int J Heat Mass Transf*. 1975;18: 1433–1441.
26. Zhang D, Mujumdar AS. Deformation and stress analysis of porous capillary bodies during intermittent volumetric thermal drying. *Drying Technol*. 1992;10:421–443.
27. Marshall MG, Metaxas AC. Radiofrequency assisted heat pump drying of crushed brick. *Appl Therm Eng*. 1999;19:375–388.
28. Chou SK, Chua KJ. New hybrid drying technologies for heat sensitive foodstuffs. *Trends Food Sci Technol*. 2001;12:359–369.
29. Islam RM, Ho JC, Mujumdar AS. Simulation of liquid diffusion-controlled drying of shrinking thin slabs subjected to multiple heat sources. *Drying Technol*. 2003;21:413–438.
30. Kowalski SJ, Musielak G, Banaszak J. Experimental validation of the heat and mass transfer model for convective drying. *Drying Technol*. 2007;25:107–121.
31. Musielak G, Banaszak J. Non-linear heat and mass transfer during convective drying of kaolin cylinder under non-steady conditions. In: Kowalski SJ, editor. *Drying of Porous Materials*. Dordrecht, The Netherlands: Springer, 2007:121–134.
32. Kowalski SJ. *Thermomechanics of Drying Processes*. Berlin-Heidelberg-New York: Springer-Verlag, 2003.
33. Kowalski SJ. Continuous thermohydromechanical model using the theory of mixtures. In: Tsotsas E, Mujumdar AS, editors. *Modern Drying Technology*, Vol. 1. Weinheim: Wiley-VCH Verlag GmbH & Co. KGaA, 2007:125–154.
34. Perre P, Remond R, Turne IW. Comprehensive drying models based on volume averaging: background, application and perspective. In: Tsotsas E, Mujumdar AS, editors. *Modern Drying Technology*, Vol. 1. Weinheim: Wiley-VCH Verlag GmbH & Co. KGaA, 2007:1.
35. Couture F, Bernada P, Roques MA. Continuous thermomechanical models using volume-averaging theory. In: Tsotsas E, Mujumdar AS, editors. *Modern Drying Technology*, Vol. 1. Weinheim: Wiley-VCH Verlag GmbH & Co. KGaA, 2007:103.
36. Bowen RM. Compressible porous media models by use of the theory of mixtures. *Int J Eng Sci*. 1982;20:697–735.
37. Gumiński K. Thermodynamic of Irreversible Processes. Warszawa: PWN-Polish Scientific Publishers, 1962 (in Polish).
38. Szarawara J. *Chemical Thermodynamics*. Warszawa: WNT-Scientific Technological Publishers, 1985 (in Polish).
39. Hill JM, Marchant TR. Modelling microwave heating. *Appl Math Model*. 1996;20:3–15.
40. Di P, Chang DPY, Dwyer HA. Heat and mass transfer during microwave steam treatment of contaminated soils. *J Environ Eng*. 2000;12:1108–1115.
41. Ratanadecho P, Aoki K, Akahori M. Experimental and numerical study of microwave drying in unsaturated porous material. *Int Commun Heat Mass Transf*. 2001;28:605–616.
42. Ratanadecho P, Aoki K, Akahori M. A numerical and experimental investigation of the modelling of microwave melting of frozen packed beds using a rectangular wave guide. *Int Commun Heat Mass Transf*. 2001;28:751–762.
43. Rajagopal KR, Tao L. Modeling of the microwave drying process of aqueous dielectrics. *Z Angew Math Phys*. 2002;53:923–948.
44. Strumiłło Cz. *Foundations of Theory and Technology of Drying*, 2nd ed. Warszawa: WNT-Scientific Technological Publishers, 1983 (in Polish).
45. Scherer GW. Theory of drying. *J Am Ceram Soc*. 1990;73:1–14.
46. Kneule F. *Drying*. Warszawa: Arkady, 1970 (in Polish).
47. Kowalski SJ, Rybicki A. The vapor-liquid interface and stresses in dried bodies. In: Kowalski SJ, editor. *Drying of Porous Materials*. Dordrecht, The Netherlands: Springer, 2007:43–58.
48. Musielak G. Modelling of the heat and mass transport phenomena in kaolin during the first and the second periods of drying. *Chem Process Eng*. 2004;25:393–409 (in Polish).
49. Pikoń J, Hehlmann J, Sąsiadek B, Janowicz R. *Chemical Apparatus*. Gliwice: Silesian University of Technology, 1972 (in Polish).
50. Wiśniewski S, Wiśniewski TS. *Heat Exchange*, 4th ed. Warszawa: WNT-Scientific Technological Publishers, 1997 (in Polish).
51. Banaszak J. Determination of the effective thermal conductivity coefficient for dried material. In: Kowalski SJ, editor, *Proceedings of the XI Polish Drying Symposium*, Poznań, Poland, 2005.
52. Musielak G, Banaszak J, Kasperek J. Determination of the temperature dependence of diffusion coefficient in fully saturated kaolin. In: Kowalski SJ, editor, *Proceedings of the XI Polish Drying Symposium*, Poznań, Poland, 2005.
53. Musielak G. Numerical treatment of non-linear boundary condition of convective mass transfer during drying, In: Farkas I, editor, *Proceedings of 15*th *International Drying Symposium* (IDS), Vol. A. Budapest, Hungary, 2006:336–342.

Manuscript received Oct. 24, 2008, revision received Apr. 16, 2009, and final revision received Apr. 21, 2009.